Jurnal Asiimetrik: Jurnal Ilmiah Rekayasa Dan Inovasi
Terakreditasi "**Peringkat 3**" berdasarkan SK Dirjendiktiristek, Nomor: 225/E/KPT/2022
Volume 6 Nomor 2 Tahun 2024, Juli 2024, Halaman 327-340
Website : http://journal.univpancasila.ac.id/index.php/asiimetrik/

p-ISSN 2655-1861
e-ISSN 2716-2923

Optimization of Dehumidification Air Flow Distribution in Temulawak Tray Dryer with Computational Fluid Dynamics

Optimasi Distribusi Aliran Udara Dehumidifikasi pada Pengering Temulawak Tipe Tray dengan Computational Fluid Dynamics

Ridwan*, Farul Apriansa, Rudi Irawan
Gunaradarma University, Jl. Margonda Raya No. 100 Kelurahan Pondok Cina, Kecamatan Beji, Depok 16424, Indonesia

Article information:

Received:
26/05/2024
Revised:
10/06/2024
Accepted:
23/06/2024

Abstract

Temulawak (Curcuma xanthorrhiza Roxb.), a member of the Zingiberaceae family, has long been recognized as a medicinal plant with a moisture content approximately 80-90%. The high moisture content of temulawak renders it challenging to store for extended periods without drying. Temulawak is susceptible to heat damage due to the potential for thermal degradation of its internal components. Accordingly, it can be concluded that low-temperature and low-air-humidity drying conditions are required. Furthermore, one of the most suitable methods is the use of a dryer that incorporates a dehumidification process. The objective of this research is to develop a temulawak dryer design and simulation variations of the incoming velocity of air flow to obtain the most optimal drying chamber by incorporating a vertical airflow channel. A design and simulation for a temulawak dryer were created using the 2022 version of SolidWorks software (flow simulation modul). The design started from drawing two-dimension, then three-dimension, and determining boundary condition and meshing. A fluid temperature of 35.7°C and a relative humidity (RH) of 22% were used to model the drying process at varying airflow velocities of 1.5 m/s, 2 m/s, and 2.5 m/s. The drying chamber, with dimensions of 676 mm x 406 mm and height of 806 mm, was designed using the type AISI 304 and achieved the most optimal airflow distribution results at a velocity of 2.5 m/s, exhibiting a relatively higher fluid temperature than the other two airflow velocity variation.

Keywords: *air distribution*, tray dryer, CFD.

***SDGs*:**

Abstrak

Temulawak (*Curcuma xanthorrhiza Roxb.*), yang termasuk ke dalam famili *Zingiberaceae*, telah lama dikenal dan banyak dimanfaatkan sebagai tanaman obat, dengan kadar air sekitar 80-90%. Tingginya kadar air ini membuat temulawak sulit untuk disimpan dalam jangka waktu yang lama tanpa proses pengeringan. Temulawak sensitif terhadap panas karena akan merusak kandungan di dalamnya. Maka, diperlukan kondisi pengeringan dengan suhu rendah dan kelembaban udara rendah, dan salah satu metode pengeringan yang cocok adalah pengering dengan metode dehumidifikasi. Tujuan penelitian ini menghasilkan rancangan alat pengering temulawak dan variasi kecepatan aliran udara masuk pada ruang pengering yang paling optimal dengan menambahkan *Vertical Airflow Channel*. Perancangan desain dan simulasi alat pengering temulawak menggunakan software solidworks 2022 (modul simulasi aliran). Perancangan dimulai dari penggambaran dua-dimensi, kemudian tiga-dimensi, serta menentukan kondisi batas dan meshing. Pemodelan dengan memvariasikan kecepatan aliran udara 1.5 m/s, 2 m/s, dan 2.5 m/s menggunakan temperatur fluida 35.7 °C dan *relative humidity* (RH) 22 %. Ruang pengering yang dirancang dengan dimensi sebesar 676 mm x 406 mm dan tinggi ruang pengering 806 mm menggunakan jenis material AISI 304 mendapatkan hasil simulasi distribusi aliran udara yang paling baik pada kecepatan 2.5 m/s dengan *temperature (fluid)* yang relatif lebih baik dibandingkan 2 variasi kecepatan aliran udara lainnya.

Kata Kunci: distribusi udara, *tray dryer*, CFD.

*Correspondence Author
email : ridwan@staff.gunadarma.ac.id

1. INTRODUCTION

Temulawak (Curcuma xanthorrhiza Roxb.), a member of the Zingiberaceae family, has a long history of medicinal use. Fresh temulawak exhibits a moisture content of approximately 75%-80%bb, rendering it susceptible to deterioration when it is stored in large quantities due to its high moisture content (Suryanantha, Yulianti and Sulastri, 2022). The high moisture content of temulawak renders it susceptible to deterioration when stored for extended periods without a drying process. In general, dried medicinal materials are stored in the form of simplisia (Santoso *et al.*, 2023). It is essential to employ a drying process to ensure the quality production of temulawak simplisia. Temulawak, as a natural ingredient utilized in the preparation of medicinal products, is not subjected to any additional processing beyond the drying process. The potential for developing temulawak as a functional food is considerable high, given its ease of cultivation and the health benefits it offers (Sihite and Hutasoit, 2023).

One of the most commonly employed techniques for the preservation of materials is drying. This process is an integral step in the post-harvest processing of agricultural products (Sudirman *et al.*, 2023). The primary objective of drying is to reduce the moisture content of the material to a specified level, thereby minimizing the risk of damage due to microbial and chemical reactions. It allows to maintain the quality of the dried product (Putra and Kuncoro, 2021). The pivotal role of the drying process in determining the quality of temulawak simplisia cannot be overlooked. The significance of selecting an appropriate drying method is underscored, as the process can reduce the moisture content to prevent the deterioration of temulawak quality. The drying process can influence the levels of chemical compounds and the pharmacological effects contained in medicinal plants, particularly for those with antioxidant properties (Pratiwi and Wardaniati, 2019).

One of the methods employed is dehumidification drying, in which the water content of solid materials is transferred using heat as an energy source. The drying of air with a low relative humidity facilitates the drying process. This method employs a refrigeration system for air temperature conditioning (Hidayati, Baharuddin and Wahyudi, 2020). Low relative humidity of the air ultimately favors the water from the materials being dried (Putra and Kuncoro, 2021). Dehumidifier dryers offer several advantages over conventional dryers. They are more hygienic, as well as easier to control of air temperature and humidity. This versatility allows them to be used in a wide range of cooled or heated temperature ranges (Akhtar *et al.*, 2024). Additionally, products dried using dehumidifiers are better quality, do not depend on external weather conditions, and do not produce fumes that can pollute the atmosphere (Abeyrathna, Ekanayake and Amaratunga, 2020). The color and aroma of products produced through dehumidifier drying are superior to those produced through high temperature drying (Liu *et al.*, 2022). An increase in temperature leads to a decrease in moisture content and simultaneously decreases curcumin content, and vice versa. Drying using a dehumidification system is more recommended than sun drying, as the dried product has a superior physical appearance and is hygienic.

The relationship between air humidity and temperature in the drying process indicates that at low temperatures, air humidity tends to be high, and conversely, at high temperatures, air humidity will be low. However, in the drying of herbal materials, the use of high temperatures is undesirable as it can result in voids and damage the active ingredients contained in the dried material (Sukmawati and Merina, 2019). Conversely, drying at low temperatures with high air humidity will necessitate a lengthy drying period, which may result in the deterioration of the herbal materials. Therefore, drying conditions with low temperature and low air humidity are required, and the potential solution is a dehumidification dryer (Putra and Kuncoro, 2021).

In addition, the geometry or shape of the drying chamber has an impact on the quality and uniformity of the material being (Haryanto, Sutoyo and Sutisna, 2019). The choice of dryer type is also something that must be considered. The use of a tray dryer has many advantages, but

on the other hand, the tray dryer has a weakness, where the tendency of the bottom tray and the top tray is less hot (Putri *et al.*, 2021). It is because hot air has passed through the bottom tray, where commodities are located, and the top tray only receives the remaining air from the previous drying process. The level of drying uniformity is strongly influenced by the airflow pattern, which can be optimized through the use of Computational Fluid Dynamics (CFD) simulation. Therefore, to improve the performance of the device, it is essential to understand the airflow pattern within the dryer.

A primary advantage of computational fluid dynamics (CFD) is that it enables the prediction of the distribution of airflow, velocity, and temperature, as well as the evaluation of changes in fluid flow modeling and the optimal design of industrial processes (Asadbeigi *et al.*, 2023). Therefore, the development of a dryer that employs the dehumidifier method to accelerate the drying process while maintaining product quality is necessary. In addition, the geometry of the drying chamber must be considered carefully in this tool, necessitating related research. The objective of this research is to develop a temulawak dryer design and to study the variations of the incoming velocity of the air flow in the most optimal drying chamber by adding a vertical airflow channel. It is, therefore, anticipated that the findings of this study will enhance the efficacy and quality of temulawak drying by elucidating the airflow pattern within the drying chamber through the incorporation of a vertical airflow channel, employing the computational fluid dynamics (CFD) method. The results will ultimately contribute to the advancement of food security and the advancement of the broader industrial sector.

2. METHODOLOGY

2.1. Flowchart

The research flow chart is presented in the Figure 1. This flow chart generally shows the design steps and computational fluid dynamics analysis steps that was conducted in this research. Starting from problem identification, literature study, making designs and running simulations. The last is to analyze the data and discuss the results of this research.

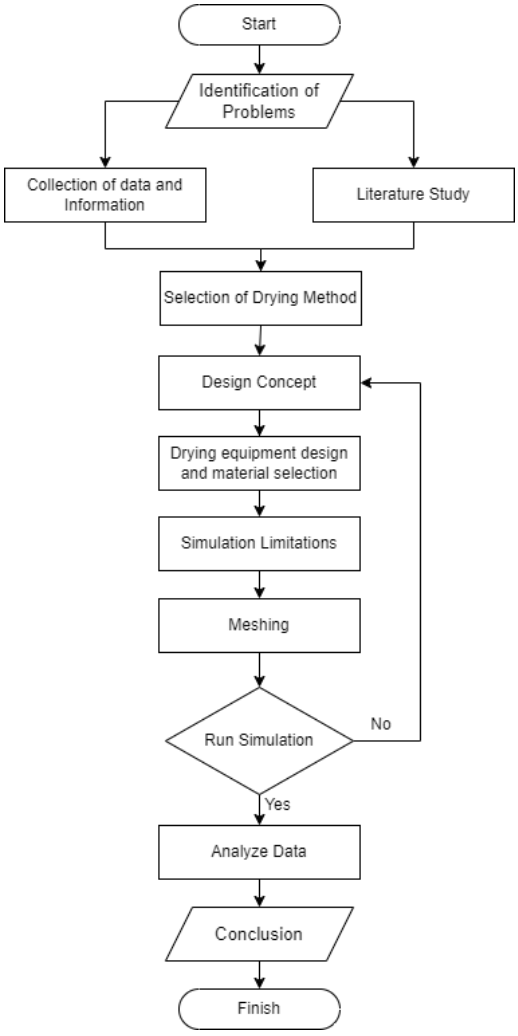

Figure 1. Research flowchart.

2.2. Research Location

In this research, the design and simulation process and data collection were carried out at the Engineering Drawing Laboratory of the Department of Mechanical Engineering, Faculty of Industrial Technology, Gunadarma University.

2.3. Research Equipment and Materials

2.3.1. Hardware

The laptop that was used in this research must have had specifications capable of running Solidworks software. The laptop used has specifications, Intel Core i5-10300H CPU 2.50GHz processor, VGA GeForce GTX 1650 Ti, 8 GB RAM, 64-bit operating system, Windows 11.

2.3.2. Software

In this research, Solidworks 2022 software was used to design and simulate fluid flow in the drying chamber.

2.4. Drying Scheme

The drying scheme employs a dehumidification method, whereby environmental air is drawn into the dehumidifier chamber, where it passes through evaporators and condensers before being sucked by the blower. This process serves to condition the air humidity and increases the air temperature (Putra and Kuncoro, 2021). Once the air has been sucked, the blower then blows the dehumidified air into the drying room. The drying room has a vertical airflow channel that helps to ensure that each tray receives the same air composition. At this point, the dehumidified air passes through the tray in the drying room, where it dries the commodity (temulawak) that is on the tray. Additionally, the air is released through the exhaust in the drying chamber. Figure 2 provides an illustration of the drying scheme.

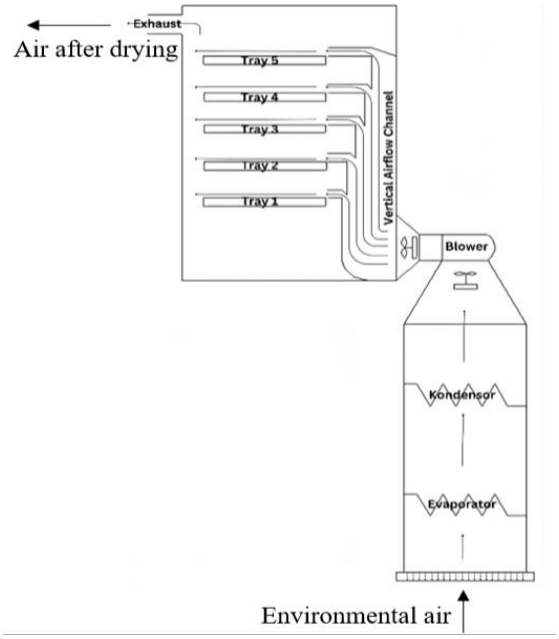

Figure 2. Drying scheme.

2.5. Drying Chamber Components

The drying chamber has main components including Vertical Airflow Channel and tray geometry as described in Figure 3 The tray dryer has a weakness which is the temperature tendency on the bottom tray and the top tray is uneven. Therefore, it is very important to know the airflow and air velocity in the drying room, so as to know the areas with adequate air velocity for proper drying. The Vertical Airflow Channel aims to concentrate the airflow which is directed directly to each tray which is arranged vertically.

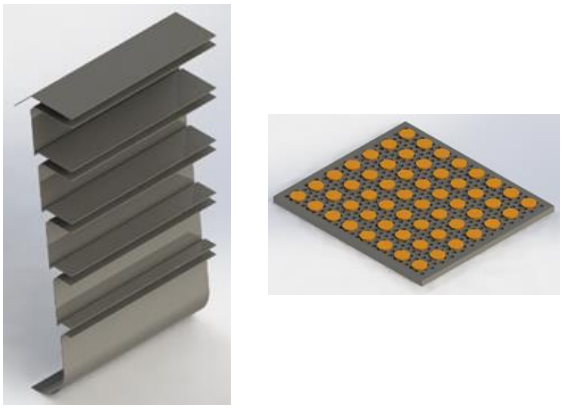

(a) Vertical airflow (b) Tray

Figure 3. Drying chamber components.

This vertical airflow channel is formed from a plate that is bent with a thickness of 2 mm using AISI 304 material. AISI 304 is a stainless material commonly used in the food and beverage industry (Sungkono and Ismarwanti, 2021). The plate is bent so that the air can be distributed in a focused manner on each tray, as shown in Figure 3a. It is our hope that the addition of this vertical airflow channel results in each tray receiving an identical air composition, thereby maintaining the quality of the dried temulawak. The tray serves as a place to place the material to be dried. The tray is arranged vertically with dimensions of 450 mm x 400 mm with a hole diameter of 10 mm. Figure 3b shows a tray with commodities placed on it. This is done to observe the flow pattern when the tray is filled with temulawak later on. The commodities are made to resemble temulawak with a thickness of 3 mm. When drying temulawak later, they will be sliced as shown in Figure 3.

In Figure 4, the dimensions of the Vertical Airflow Channel are made by providing 10 mm backward at each level, thus allowing air flowing from below when heading up to enter through the gap.

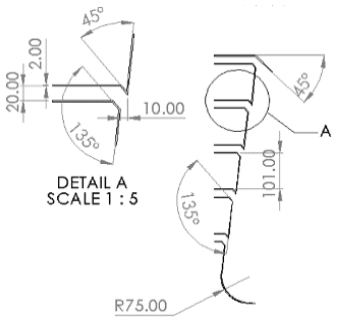

Figure 4. Dimension details of vertical airflow channel.

2.6. Boundary Condition

The fluid simulation boundary conditions presented in Table 1 serve to define the limits of the input data parameters. The temperature entering the drying chamber is not excessively high, while the relative humidity is low, in order to ensure that the air is dry. This is because temulawak is sensitive to heat, thus preventing the destruction of its contents (Putra and Kuncoro, 2021).

Table 1. Boundary condition.

Temperature (fluid)	35.7 °C (308.85 K)
Relatif humidity (RH)	22 %
Solid parameters	27.2 °C (300.35 K)

In this research, the fluid used was air with the temperature set at 35.7 °C and relative humidity 22%. This temperature was selected based on previous research (Putra and Kuncoro, 2021) which indicated that it is the most optimal temperature to avoid shrinkage rates at the beginning of drying. It is widely known that temperature affects the shrinkage rate. The higher the temperature is, the greater the shrinkage is. Since in the low-temperature drying process, shrinkage does not occur as quickly as high-temperature drying processed, the objective of the selection of 35.7 °C temperature set is to prevent shrinkage at the outset of the drying process, if shrinkage occurs too rapidly. The shrinkage of temulawak will also shrink the surface pores of temulawak which cause the water content is difficult to evaporate.

The study employs a variable airflow velocity when entering the drying chamber. The data presented in Table 2 was utilized in the simulation.

Table 2. Inlet air flow velocity variation data.

Simulation Data	Airflow Velocity (m/s)
Data 1	1.5
Data 2	2
Data 3	2.5

2.7. Meshing

After setting the simulation boundaries, the next step is to mesh the model. The mesh consists of two main types of elements: quadrilateral and triangular (Billad *et al.*, 2024). In this research, a total element of 677272 cells. The choice of quadrilateral elements was based on their ability to provide a more accurate meshing with less error compared to triangular elements, as supported by Billad et al. (Billad *et al.*, 2024). Specifically, quadrilateral elements offer better numerical stability and convergence properties, which are crucial for the precision of the simulation results.

Table 3. Analysis mesh.

Total Cells Count	677272
Fluid Cells	442623
Solid Cells	234649
Partial Cells	171382

To provide a detailed analysis of the meshing process, Table 3 presents the analysis mesh used in the simulation, including the total cell count, fluid cells, solid cells, and partial cells (see Figure 5). This table highlights the key factors considered in optimizing the mesh for accuracy and computational efficiency.

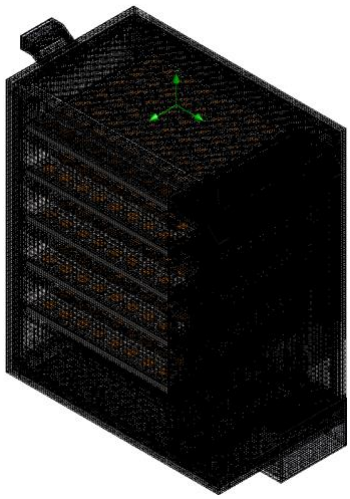

Figure 5. Meshing.

3. RESULTS AND DISCUSSION

The results and discussion present a description of the research data, which is equipped with tables and figures.

3.1. Dryer Design

The drying chamber is constructed with dimensions of 676 mm x 406 mm x 806 mm, a plate thickness of 3 mm, and a distance between trays of approximately 125 mm. The manufacturing material for this drying chamber is AISI 304. The outcomes of this design are illustrated in Figure 6.

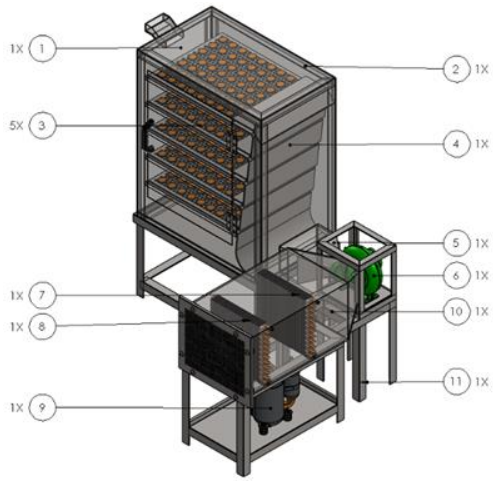

Figure 6. Dryer design.

Table 4 presents a tabular description of the apparatus depicted in Figure 6, which is used for the drying of temulawak using the dehumidification method. It includes the number of components in the tray dryer.

Table 4. Partlist component.

No Balloon	Part Name	Quantity
1	Drying chamber	1
2	Drying chamber frame	1
3	Tray	5
4	VerticalAirflow Channel	1
5	Adapter	1
6	Blower	1
7	Condensor	1
8	Evaporator	1
9	Compressor	1
10	Dehumidifier Chamber	1
11	Dryer Frame	1

3.2. Temperature (Fluid)

The simulation results demonstrate the color contours of the temperature distribution in the drying chamber at varying air velocities at the inlet, specifically 1.5 m/s, 2 m/s, and 2.5 m/s. The air temperature utilized in the simulation was 35.7°C (308.65 K), relative humidity (RH) 22%, and solid parameters 27.2°C (300.35 K). The results are presented in the form of a color contour cut plot of the front view and for each tray.

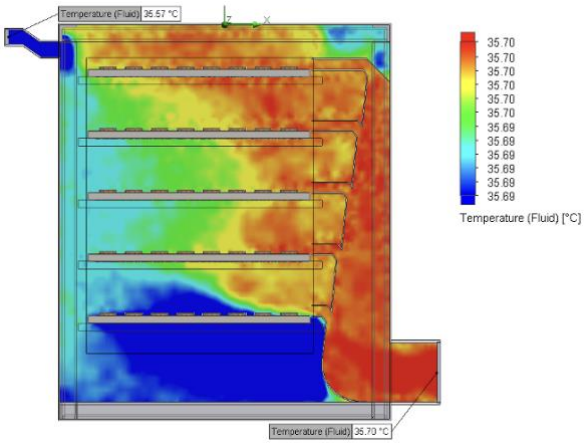

Figure 7. Temperature distribution results with an inlet airflow velocity of 1.5 m/s.

In Figure 7, the temperature difference within the drying chamber is observed between the inlet and outlet values, measuring 0.13 °C with an inlet temperature of 35.70 °C and an outlet temperature of 35.57 °C.

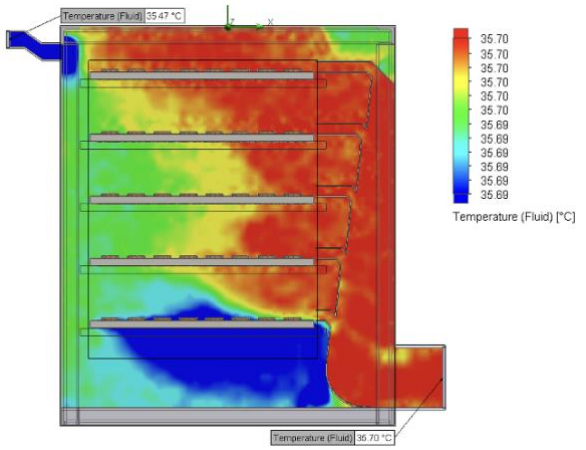

Figure 8. Temperature distribution results with an inlet airflow velocity of 2 m/s.

In Figure 8, the temperature difference within the drying chamber is observed between the inlet and outlet values, measuring 0.23 ˚C with an inlet temperature of 35.70 ˚C and an outlet temperature of 35.47 ˚C.

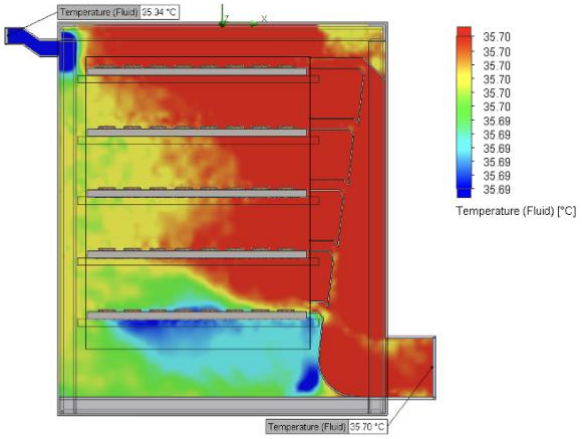

Figure 9. Temperature distribution results with an inlet airflow velocity of 2.5 m/s.

In Figure 9, the temperature difference within the drying chamber is observed between the inlet and outlet values, measuring 0.36 ˚C with an inlet temperature of 35.70 ˚C and an outlet temperature of 35.34 ˚C. Figure 7, Figure 8, and Figure 9 demonstrate that the temperature distribution is relatively uniform at an inlet air velocity of 2.5 m/s, in comparison to the temperature variations observed at inlet air velocities of 1.5 m/s and 2 m/s. It is evident that the inlet air velocity exerts a significant influence on the temperature changes (Biksono *et al.*, 2022).

The results of the average value of fluid temperature distribution value at each variation of the inlet air flow velocity are presented in Table 5.

Table 5. Average value of temperature (fluid).

Variation of Inlet Air Flow Velocity	Unit	Value
1.5 m/s	[˚C]	35.6952
2 m/s	[˚C]	35.6964
2.5 m/s	[˚C]	35.6979

The temperature distribution in each tray is illustrated in Figure 10, Figure 11, and Figure 12, which depict color contour cut plots. Table 6 provides the data necessary to create a graph, as shown in Figure 13.

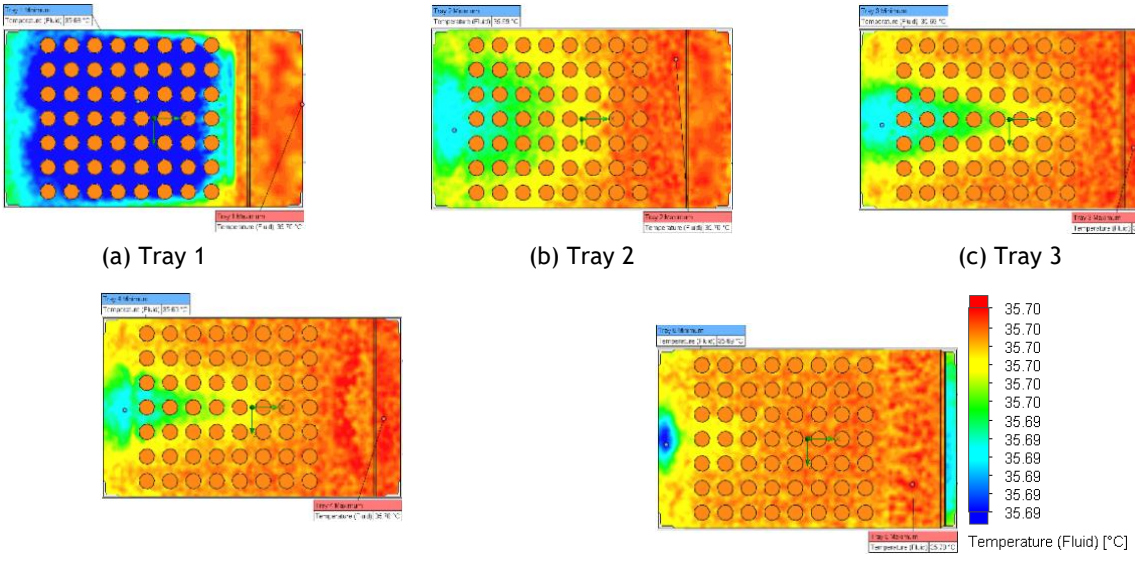

(a) Tray 1 (b) Tray 2 (c) Tray 3

(d) Tray 4 (e) Tray 5

Figure 10. Cut plot temperature (fluid) with airflow velocity 1.5 m/s.

This graph displays the results of the minimum and maximum values for fluid temperature with an inlet air flow velocity of 1.5 m/s in each tray (Figure 13).

Table 7 provides the data necessary to create a graph as shown in Figure 14. This graph displays the results of the minimum and maximum values

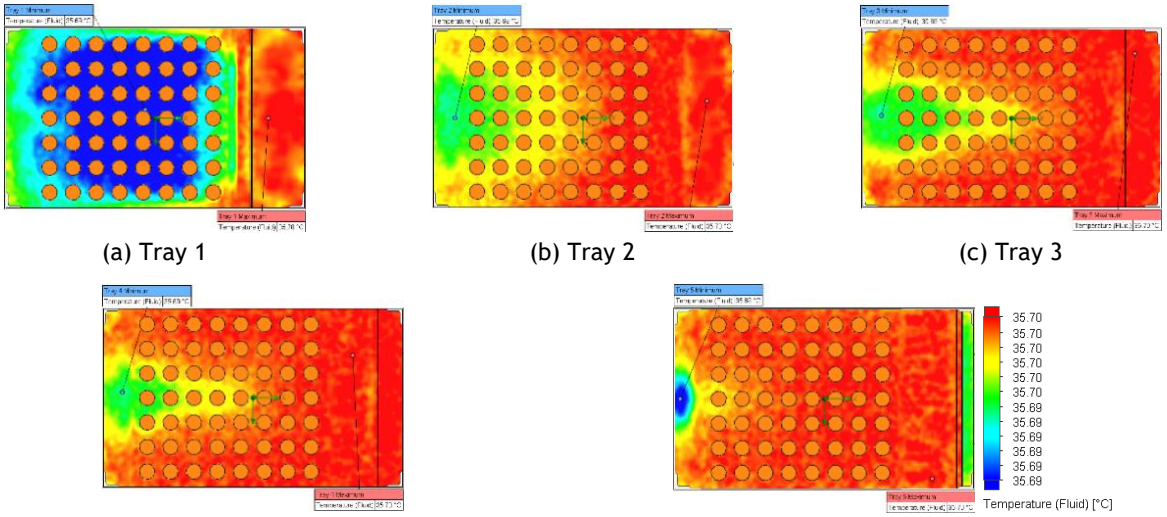

(a) Tray 1 (b) Tray 2 (c) Tray 3

(d) Tray 4 (e) Tray 5

Figure 11. Cut plot temperature (fluid) with airflow velocity 2 m/s.

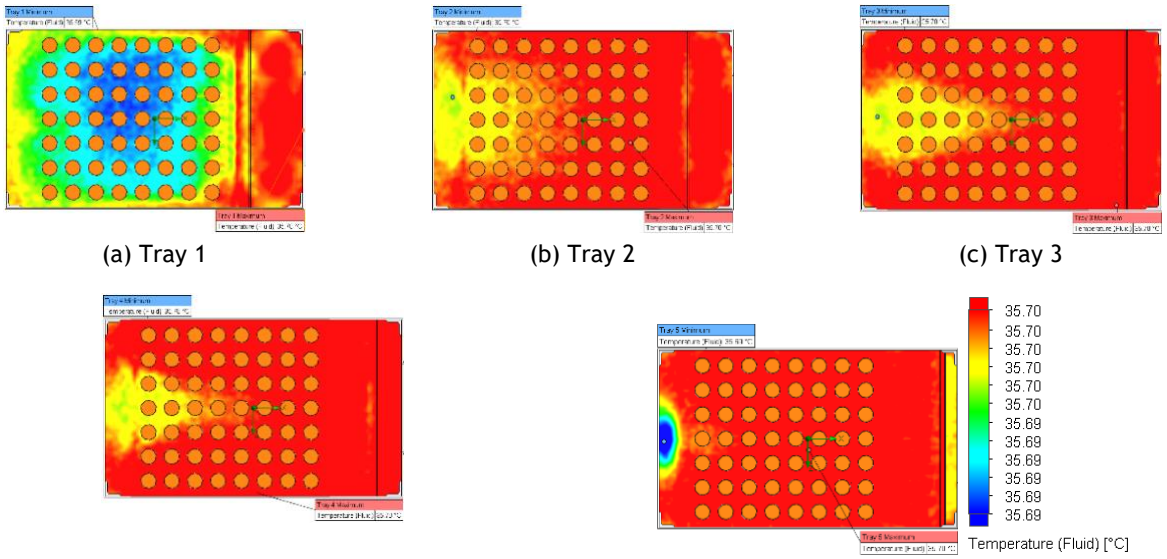

(a) Tray 1 (b) Tray 2 (c) Tray 3

(d) Tray 4 (e) Tray 5

Figure 12. Cut plot temperature (fluid) with airflow velocity 2.5 m/s.

for fluid temperature with an inlet air flow velocity of 2 m/s in each tray.

Table 6. Min and max tempetrature (fluid) values in each Tray with a air flow velocity of 2 m/s.

Tray	Minimum	Maximum
Tray 1	35.69 °C	35.70 °C
Tray 2	35.69 °C	35.70 °C
Tray 3	35.69 °C	35.70 °C
Tray 4	35.69 °C	35.70 °C
Tray 5	35.69 °C	35.70 °C

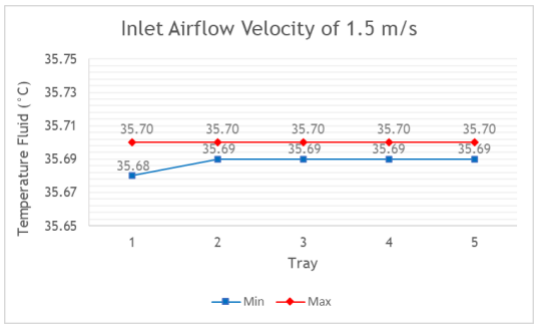

Figure 13. Graph of the fluid temparetur value with an inlet airflow velocity of 2 m/s in each tray.

Figure 11 depicts the temperature distribution across each tray. Based on the color contour cut plot, the lowest distribution is observed in tray 1 relative to the other trays. However, the temperature distribution at a velocity of 2 m/s is superior to that at a velocity of 1.5 m/s. Table 7 presents the min and max temperature values observed in each tray with an inlet air flow velocity of 2 m/s.

Table 7. Min and max tempetrature (fluid) values in each Tray with a air flow velocity of 2 m/s.

Tray	Minimum	Maximum
Tray 1	35.69 °C	35.70 °C
Tray 2	35.69 °C	35.70 °C
Tray 3	35.69 °C	35.70 °C
Tray 4	35.69 °C	35.70 °C
Tray 5	35.69 °C	35.70 °C

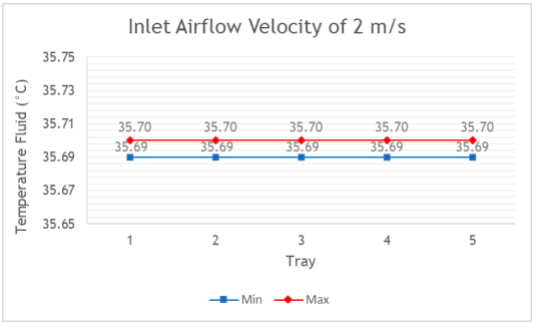

Figure 14. Graph of the fluid temparetur value with an inlet airflow velocity of 2 m/s in each tray.

Table 8. Min and max tempetrature (fluid) values in each Tray with a air flow velocity of 2.5 m/s.

Tray	Minimum	Maximum
Tray 1	35.69 °C	35.70 °C
Tray 2	35.70 °C	35.70 °C
Tray 3	35.70 °C	35.70 °C
Tray 4	35.70 °C	35.70 °C
Tray 5	35.69 °C	35.70 °C

Table 8 provides the data necessary to create a graph, as shown in Figure 15. This graph displays the results of the minimum and maximum values for fluid temperature with an inlet air flow velocity of 2.5 m/s in each tray.

Figure 12 illustrates the temperature distribution across each tray. The color contour cut plot indicates that the lowest distribution is observed on tray 1 in comparison to the other trays. However, the temperature distribution at a velocity of 2.5 m/s is superior to those at 1.5 m/s and 2 m/s. It can be observed from the color contour cutplot in each tray that the temperature distribution at this velocity is superior to those at the other velocities. It can be demonstrated that the inlet air velocity exerts a significant influence on the temperature changes (Biksono *et al.*, 2022).

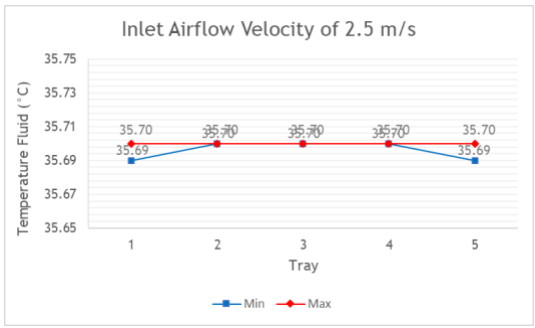

Figure 15. Graph of the fluid temparetur value with an inlet airflow velocity of 2.5 m/s in each tray.

The min and max temperature values in each tray with an airflow velocity of 2.5 m/s can be found in Table 8. Table 8 indicates that the min and max values at an inlet airflow velocity of 2.5 m/s are observed in trays 2, 3, and 4, where the min and max air temperatures remain at 35.7 °C. This indicates that the air flow velocity of 2.5 m/s is superior to the velocity variations of 1.5 m/s and 2 m/s.

3.3. Velocity

The simulation results demonstrate the color contours of the air distribution within the drying chamber at varying air velocities at the inlet, specifically 1.5 m/s, 2 m/s, and 2.5 m/s. The air temperature utilized in the simulation was 35.7°C (308.85 K), the relative humidity (RH) was 22%, and the solid parameters were 27.2°C (300.35 K). The results are presented in the form of a color contour cut plot of the front view and for each tray.

In Figure 16, the airflow velocity difference within the drying chamber is observed between the inlet and outlet values, measuring 14.630 m/s with an inlet airflow velocity of 1.5 m/s and an outlet value of 16.130 m/s. In Figure 17, the airflow velocity difference within the drying chamber is observed between the inlet and outlet values, measuring 19.571 m/s with an inlet airflow velocity of 2 m/s and an outlet value of

21.571 m/s. In Figure 18, the airflow velocity difference within the drying chamber is observed between the inlet and outlet values, measuring 24.352 m/s with an inlet airflow velocity of 2.5 m/s and an outlet value of 26.852 m/s.

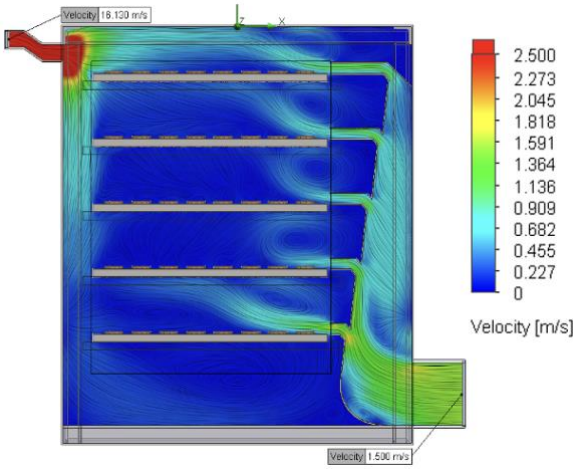

Figure 16. Air dispersion results with an inlet airflow velocity of 1.5 m/s.

Figure 16, Figure 17, and Figure 18 illustrate the outcomes of the cut plot color contour for each variation of air velocity entering the drying chamber (see Table 9). The cut plot indicates that an increase in air velocity entering the drying chamber is associated with an elevated air movement within it.

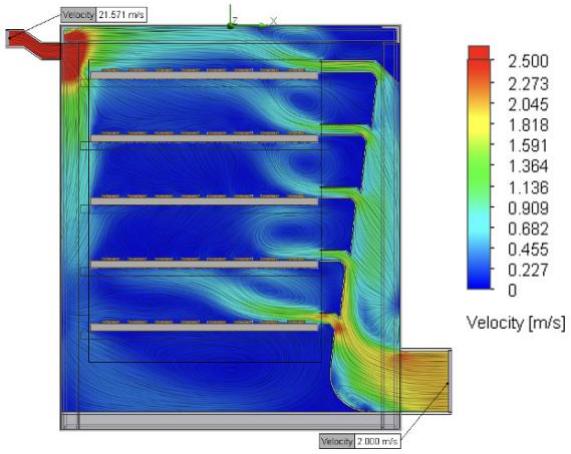

Figure 17. Air dispersion results with an inlet airflow velocity of 2 m/s.

The air distribution in each tray is illustrated in Figure 20, Figure 21, and Figure 22, which depict color contour cut plots and streamlines.

Table 10 provides the data necessary to create a graph, as shown in Figure 19. This graph displays the results of the minimum and maximum values for air distribution with an inlet air flow velocity of 1.5 m/s in each tray.

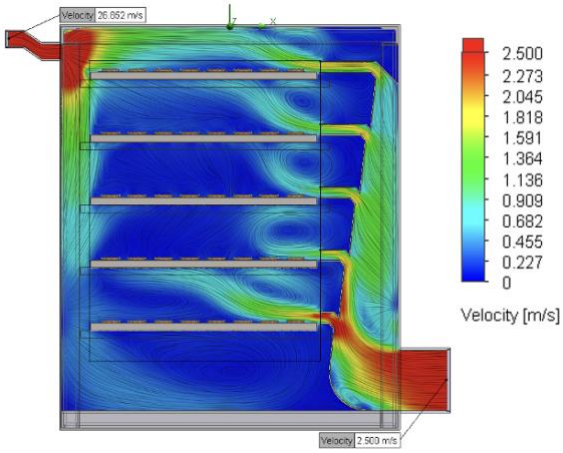

Figure 18. Air dispersion results with an inlet airflow velocity of 2.5 m/s.

Table 9. Average value of air velocity.

Variation of Inlet Air Flow Velocity	Unit	Value
1.5 m/s	[m/s]	0.3441
2 m/s	[m/s]	0.4611
2.5 m/s	[m/s]	0.5794

Table 10. Min and max values of air distribution with an inlet airflow velocity of 1.5 m/s.

Tray	Minimum	Maximum
Tray 1	0.005 m/s	1.759 m/s
Tray 2	0.006 m/s	1.336 m/s
Tray 3	0.011 m/s	1.146 m/s
Tray 4	0.013 m/s	1.195 m/s
Tray 5	0.00008294 m/s	2.769 m/s

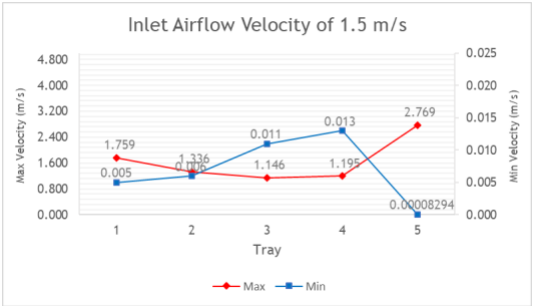

Figure 19. Graph of the air distribution value with an inlet airflow velocity of 1.5 m/s in each tray.

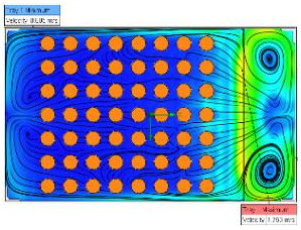

(a) Tray 1

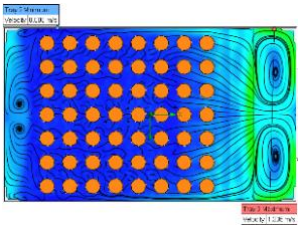

(b) Tray 2

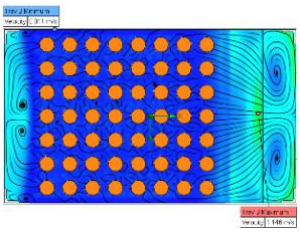

(c) Tray 3

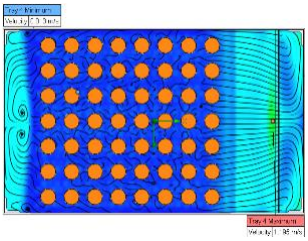

(d) Tray 4

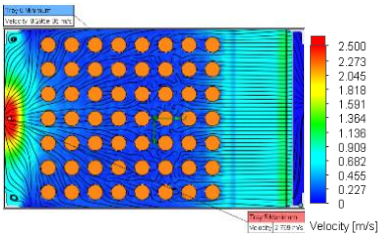

(e) Tray 5

Figure 20. Air distribution results with an inlet airflow velocity of 1.5 m/s.

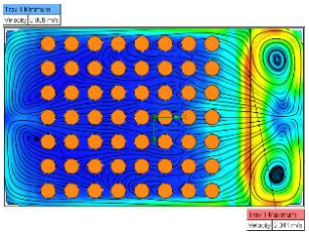

(a) Tray 1

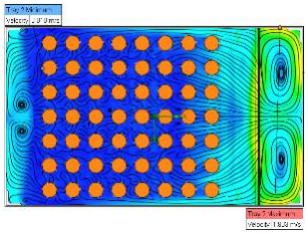

(b) Tray 2

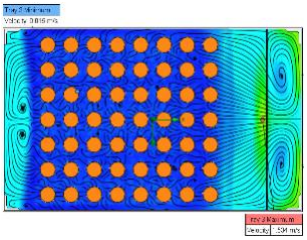

(c) Tray 3

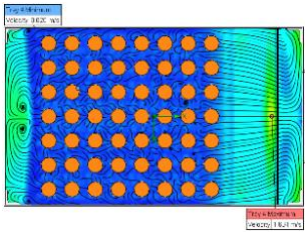

(d) Tray 4

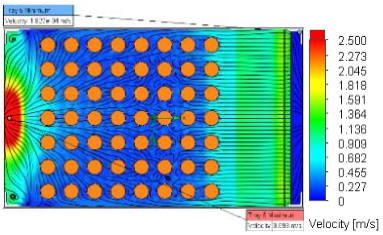

(e) Tray 5

Figure 21. Air distribution results with an inlet airflow velocity of 2 m/s.

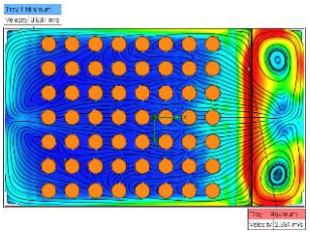

(a) Tray 1

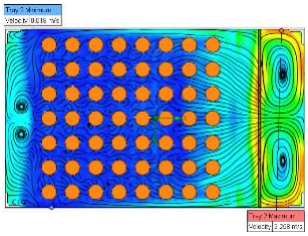

(b) Tray 2

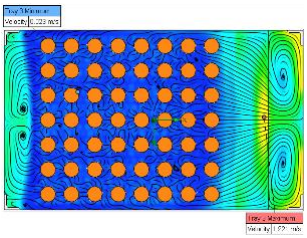

(c) Tray 3

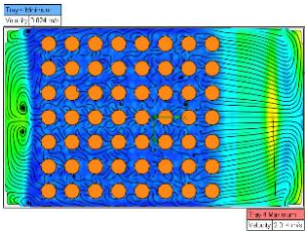

(d) Tray 4

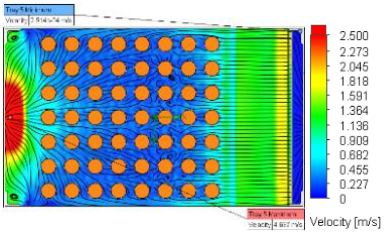

(e) Tray 5

Figure 22. Air distribution results with an inlet airflow velocity of 2.5 m/s.

Figure 20 illustrates the air distribution process at an air velocity of 1.5 m/s. The air entering the drying chamber passes through the commodity above the tray, as shown by the streamline contour. Visualization of the streamline contour makes it easier to observe the phenomenon (Billad *et al.*, 2024). By understanding the phenomena that occur, it is possible to observe the distribution of airflow patterns that occur around the tray. The illustration of the figure demonstrates that the air, upon passing through the commodity positioned on the tray, becomes randomly oriented and moves towards the exhaust. The Vertical Airflow Channel function plays a role in this process, where dry air is concentrated in each tray and passes over the commodity. The min and max velocity values at each tray with an inlet airflow velocity of 1.5 m/s are presented in Table 10.

Tray 5 exhibits a markedly lower minimum fluid velocity than the other trays, with a value of 0.00008294 m/s evident in the illustration in Figure 19. This observation is corroborated by the results presented in Figure 20, which demonstrate that the minimum probe is situated in the vicinity of the wall of the drying chamber, where the airflow is not influenced by the exhaled airflow. This is because the airflow entering the inlet will tend to move towards the exhaust. Consequently, the position of the minimum probe is inversely proportional to the exit of the air flow, which ultimately leads to the exhaust.

The observed air velocity of 0.00008294 m/s falls within the boundary layer velocity spectrum. This modest velocity indicates the proximity of the airflow to the solid boundary, where the influence of air viscosity is most pronounced. Furthermore, the velocity is close to negligible levels due to the no-slip conditions that are characteristic of airflow near solid surfaces.

Table 11 provides the data necessary to create a graph, as shown in Figure 23. This graph displays the results of the minimum and maximum values for air distribution with an inlet air flow velocity of 2 m/s in each tray.

In Figure 21 and Figure 23, illustrates the air distribution process for an inlet airflow velocity of 2 m/s. The air entering the drying chamber passes through the commodity on the tray, as indicated by the streamlines. After passing through the commodity, the fluid flow becomes random and moves towards the exhaust. The function of the Vertical Airflow Channel plays a role in this process, where the dry air is centered in each tray and passes through the commodity. Table 11 presents the min and max velocity values in each tray with an inlet airflow velocity of 2 m/s.

Table 11. Min and max values of air distribution with an inlet airflow velocity of 2 m/s.

Tray	Minimum	Maximum
Tray 1	0.006 m/s	2.344 m/s
Tray 2	0.010 m/s	1.803 m/s
Tray 3	0.015 m/s	1.534 m/s
Tray 4	0.020 m/s	1.604 m/s
Tray 5	0.0001927 m/s	3.693 m/s

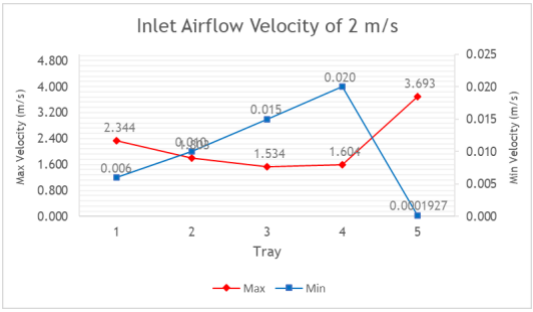

Figure 23. Graph of the air distribution value with an inlet airflow velocity of 2 m/s in each tray.

Tray 5 exhibits a markedly lower minimum fluid velocity than the other trays, with a value of 0.0001927 m/s evident in the illustration in Figure 23. This observation is corroborated by the results presented in Figure 21, which demonstrate that the minimum probe is situated in the vicinity of the wall of the drying chamber, where the airflow is not influenced by the exhaled airflow. This is because the airflow entering the inlet will tend to move towards the exhaust. Consequently, the position of the minimum probe is inversely proportional to the exit of the air flow, which ultimately leads to the exhaust.

The observed air velocity of 0.0001927 m/s is consistent with the boundary layer velocity spectrum. This relatively low velocity indicates that the airflow is in close proximity to the solid boundary, where the influence of air viscosity is most pronounced. Moreover, the velocity is close

to negligible levels due to the no-slip conditions that are characteristic of airflow near solid surfaces.

Table 12. Min and max values of air distribution with an inlet airflow velocity of 2.5 m/s.

Tray	Minimum	Maximum
Tray 1	0.007 m/s	2.934 m/s
Tray 2	0.018 m/s	2.258 m/s
Tray 3	0.023 m/s	1.921 m/s
Tray 4	0.024 m/s	2.014 m/s
Tray 5	0.0002514 m/s	4.637 m/s

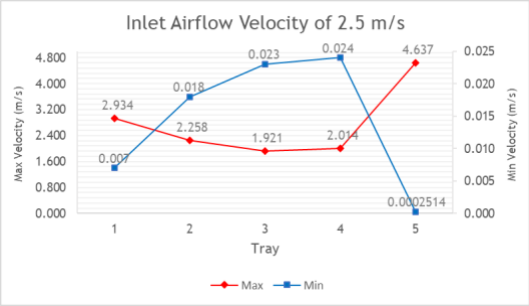

Figure 24. Graph of the air distribution value with an inlet airflow velocity of 2.5 m/s in each tray.

Table 12 provides the data necessary to create a graph, as shown in Figure 24. This graph displays the results of the minimum and maximum values for air distribution with an inlet air flow velocity of 2.5 m/s in each tray.

Figure 22 and Figure 24, illustrates the air distribution that occurs for an inlet airflow velocity of 2.5 m/s. The air entering the drying chamber and passing through the commodity on the tray can be seen in the streamlines contours. Visualization of the streamline contour makes it easier to observe the phenomenon (Billad *et al.*, 2024). By understanding the phenomena that occur, it is possible to observe the distribution of airflow patterns that occur around the tray. The figure illustrates that the air, when passing over the commodity positioned on the tray, becomes random after passing over the commodity and moves towards the exhaust. The function of the vertical airflow channel is to concentrate the dried air in each tray. The cut plot color contour results demonstrate that an increase in the air velocity entering the drying chamber is accompanied by an increase in air movement in the chamber and through the commodity. The min and max velocity values on each tray with an inlet airflow velocity of 2.5 m/s are presented in Table 12.

Tray 5 exhibits a markedly lower minimum fluid velocity than the other trays, with a value of 0.0002514 m/s evident in the illustration in Figure 24. This observation is corroborated by the results presented in Figure 22, which demonstrate that the minimum probe is situated in the vicinity of the wall of the drying chamber, where the airflow is not influenced by the exhaled airflow. This is because the airflow entering the inlet will tend to move towards the exhaust. Consequently, the position of the minimum probe is inversely proportional to the exit of the air flow, which ultimately leads to the exhaust. The observed air velocity of 0.0002514 m/s falls within the boundary layer velocity spectrum. This modest velocity indicates the proximity of the airflow to the solid boundary, where the influence of air viscosity is most pronounced. Furthermore, the velocity is close to negligible levels due to the no-slip conditions that are characteristic of airflow near solid surfaces.

The results of simulation in this research show that the geometry of the drying room affects the temperature distribution which is also shown by Haryanto et al. (Haryanto, Sutoyo and Sutisna, 2019). It means the temperature can be distributed more evenly in the drying room by adding the flow guide. The best tray for drying temulawak is tray two, compared to the other trays, because the difference between the maximum and minimum temperatures on this tray is the smallest. The result is Similar to Biksono et al., (Biksono *et al.*, 2022), this research also shows temperature distribution and flow velocity of air highly determine the quality of product. Hence, it is necessary the temperature distribution and air flow velocity are adjusted accordingly. It can be concluded that that the drying process using dehumidification can control the quality of product. Hence it is suitable as a drying method for food and medicinal plant products, such as temulawak and turmeric (Hidayati, Baharuddin and Wahyudi, 2020).

4. CONCLUSION

The drying chamber has been designed with the inclusion of trays and a vertical airflow

channel, which functions to concentrate the air flow in each tray. The dimensions of the drying chamber are 676 mm x 406 mm, with a height of 806 mm. The material type is AISI 304, and the chamber contains five trays, with a distance of 125 mm between each tray.

The drying chambers with dimensions of 676 mm x 406 mm x 806 mm, and a distance between four trays of approximately 125 mm were designed and constructed. Computational Fluid Dynamics (CFD) simulations indicate that the optimal airflow distribution in a drying chamber is achieved at a velocity of 2.5 m/s. This velocity is associated with a more optimal fluid temperature compared to the other two velocity variations. At an inflow velocity of 2.5 m/s on trays 2, 3, and 4, the temperature remains stable. The even distribution of dry air is clearly visible in the color contour, cut plot in the drying room cut plot, and in each tray at a velocity of 2.5 m/s.

REFERENCES

Abeyrathna, R.M.R.D., Ekanayake, E.M.A.C. and Amaratunga, K.S.P. (2020) 'Industrial Robotic Arm for Chilli Milling Process', *International Journal of Innovative Technology and Exploring Engineering (IJITEE)*, 9(12), pp. 130–133.

Akhtar, M.U.S. *et al.* (2024) 'Sustainable Humidity Control In The Built Environment: Recent Research And Technological Advancements In Thermal Driven Dehumidification Systems', *Energy and Buildings*, 304, p. 113846.

Asadbeigi, Sh. *et al.* (2023) 'Analyzing And Simulating Heat Transfer And Designing A Shell And Tube Heat Exchanger For The Pasteurization Process Of Tomato Paste: A CFD Study', *Heliyon*, 9(11), p. e21593.

Biksono, D. *et al.* (2022) 'Distribusi Suhu dan Kecepatan Aliran Udara dari Sistem Heat Pump Kompresi Uap untuk Ruang Pengering Tipe Drum Horizontal dengan Bantuan Computational Fluid Dynamics', *Jurnal Teknologi*, 10(1), pp. 86–99.

Billad, R.F. *et al.* (2024) 'Numerical Modelling of NACA 0015 Airfoil Under the Erosion Condition', *Jurnal Asiimetrik: Jurnal Ilmiah Rekayasa dan Inovasi*, 6(1), pp. 133–142.

Haryanto, A., Sutoyo, E. and Sutisna, S.P. (2019) 'Studi Faktor Persebaran Suhu Dan Aliran Fluida Dalam Pengering Pakaian Menggunakan Metode Numerik Dan CFD', *AME (Aplikasi Mekanika dan Energi): Jurnal Ilmiah Teknik Mesin*, 5(1), pp. 38–46.

Hidayati, B., Baharuddin and Wahyudi, R. (2020) 'Air Moisture Analysis of Potato Dehumidification Process Using The Refrigeration System', *AUSTENIT*, 12(1), pp. 1–5.

Liu, Q. *et al.* (2022) 'Comparison Of Different Drying Techniques For Shiitake Mushroom (*Lentinus Edodes*): Changes In Volatile Compounds, Taste Properties, And Texture Qualities', *LWT*, 164, p. 113651.

Pratiwi, D. and Wardaniati, I. (2019) 'Pengaruh Variasi Perlakuan (Segar dan Simplisia) Rimpang Kunyit (Curcuma domestica) Terhadap Aktivitas Antioksidan dan Kadar Fenol Total', *Jurnal Farmasi Higea*, 11(2), pp. 159–165.

Putra, A.S. and Kuncoro, H. (2021) 'Pengaruh Kondisi Pengeringan Dengan Kelembaban Dan Suhu Rendah Terhadap Penyusutan Temulawak', *Jurnal Teknologi Pertanian Andalas*, 25(1), pp. 81–89.

Putri, A.O. *et al.* (2021) 'Rancang Bangun Alat Tipe Spray Dryer Untuk Proses Pengeringan Susu Bubuk Berbasis Jagung Manis (Zea Mays Saccharata)', *KINETIKA*, 12(3), pp. 31–37.

Santoso, I. *et al.* (2023) 'Peningkatan Nilai Tambah Simplisa Jahe Merah Subgrade Di Bumdesma Sari Bumi, Kecamatan Pule, Kabupaten Trenggalek', *Journal of Innovation and Applied Technology*, 9(2), pp. 24–29.

Sihite, N.W. and Hutasoit, M.S. (2023) 'Potensi Bahan Pangan Lokal Indonesia Sebagai Pangan Fungsional Dan Manfaatnya Bagi Kesehatan :Review', *JURNAL RISET GIZI*, 11(2), pp. 133–138.

Sudirman *et al.* (2023) 'Aplikasi Cooling Dehumidification pada Mesin Pengering untuk Mengeringkan Hasil Panen Tanaman Herbal', *Jurnal Rekayasa Mesin*, 18(1), pp. 37–44.

Sukmawati, W. and Merina, M. (2019) 'Pelatihan Pembuatan Minuman Herbal Instan Untuk Meningkatkan Ekonomi Warga', *JURNAL PENGABDIAN KEPADA MASYARAKAT*, 25(4), pp. 210–215.

Sungkono and Ismarwanti, S. (2021) 'Pengaruh Perlakuan Panas Terhadap Perilaku Tarik Dan Struktur Mikro Baja Tahan Karat Aisi 304 Pada Daerah Sensitisasi 600 – 700 °C', *Urania : Jurnal Ilmiah Daur Bahan Bakar Nuklir*, 27(3), pp. 123–132.

Suryanantha, I.W., Yulianti, N.L. and Sulastri, N.N. (2022) 'Optimasi Suhu Pengeringan dan Ketebalan Irisan pada Proses Pengeringan Temulawak (Curcuma Xanthorrhiza Roxb) dengan Response Surface Methodology (RSM)', *Jurnal BETA (Biosistem dan Teknik Pertanian)*, 10(2), pp. 259–268.